



Energy absorption during failure of layered metal foam/ceramic laminates

A.E. Markaki, T.W. Clyne *

Department of Materials Science and Metallurgy, Cambridge University, Pembroke Street, Cambridge CB2 3QZ, UK

Received 15 January 2001; received in revised form 23 March 2001

Abstract

This study is concerned with the fracture behaviour of laminates made up of alternate layers of metal foam and ceramic. It is shown that the fracture energy of such material measured in flexure is broadly consistent with predictions from a model based on analysis of the plastic work done in deforming metal ligaments bridging between fractured ceramic sheets. Since the metal foams employed are rather brittle materials, the plastic work done in this mode, and hence the fracture energies of these laminates, were relatively low. Multiple cracking, which can enhance the work of fracture substantially was not observed with these laminates and this is also shown to be consistent with model predictions. The cell wall microstructure within the foam, which affects both local and global plastic deformation characteristics, is identified as an important factor. There is a need for metallic foams with cell walls exhibiting relatively high ductility and toughness. © 2002 Elsevier Science B.V. All rights reserved.

Keywords: Fracture behaviour; Metallic foams; Layered metal/ceramic systems

1. Introduction

Layered metal/ceramic systems have the potential to exhibit attractive combinations of low density with high strength, stiffness and toughness [1–6]. Energy dissipation during in-plane tensile loading and bending is dominated by plastic deformation of the metal ligaments in the crack wake which stretch as the crack opens, until they are ruptured. Furthermore, under localised loading, such as that which occurs beneath an indenter or during impact by a projectile, systems employing ceramics backed by a ductile medium can offer good ballistic performance [7,8].

If the dense metal layers are replaced by metal foams, the constraint imposed by the surrounding ceramic layers is substantially reduced, since there can be no stress normal to a free surface. A further difference will arise from changes in the stress field at the crack tip. It is expected that the stress experienced by the succeeding ceramic layer will be lower than would be the case for a fully dense metal of the same areal weight. Under

localised loading, the loss of constraint can have a profound effect on the global (out-of-plane) and local deformation of the laminates and in turn, on the impact response [9].

In the present work, laminates consisting of alternate layers of Al alloy foam and Al_2O_3 were fabricated in a vacuum hot press. In order to establish an understanding of the mechanisms by which they fail, their response under in-plane tensile and flexural loading has been investigated. Comparisons are presented between measured fracture energies during bending and predictions based on the deformation behaviour of bridging ligaments under small-scale yielding conditions. Moreover, indentation tests were carried out in order to explore their behaviour under localised loading.

2. Experimental procedures

2.1. Materials

Two closed cell Al alloy foams were used as the metallic constituent in the laminates. Cast Al–12Si–0.6Mg and wrought Al–1Mg–0.6Si aluminium alloy

* Corresponding author. Fax: +44-1223-334567.

E-mail address: twc10@cam.ac.uk (T.W. Clyne).

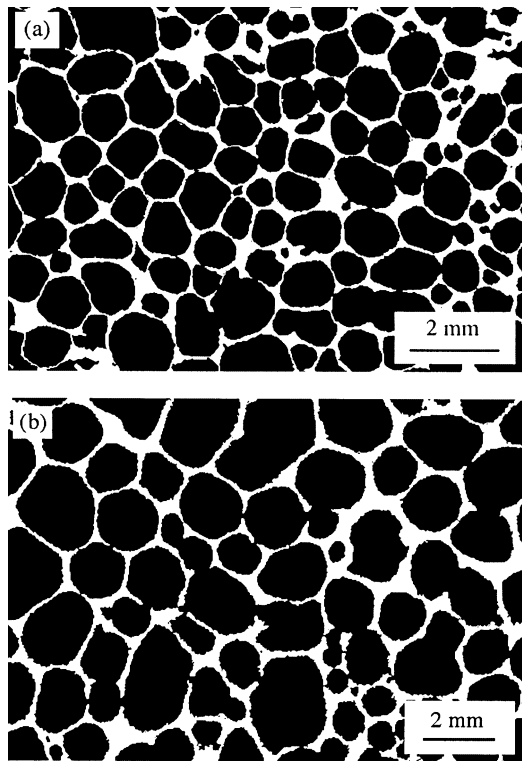


Fig. 1. Binary images showing the cell structure of the materials investigated (a) FC; and (b) FW.

foams, henceforth designated FC and FW, respectively, were produced by a powder metallurgical process [10]. Typical cell structures of the two foams are illustrated in Fig. 1. Structural parameters are listed in Table 1. Detailed characterisation of the two materials including an examination of the cell wall microstructure is presented elsewhere [11].

Two specimen geometries were employed: (i) foam/ Al_2O_3 multi-layer laminates; and (ii) foam/ Al_2O_3 sandwich specimens. The first configuration used for flexure, tension and indentation tests, consisted of four Al_2O_3 layers alternated with three foamed metal layers. Two foam layer thicknesses, h_f , of about 2 and 3 mm were used, while the Al_2O_3 layers had a constant thickness, h_c , of 1 mm. In the second configuration, the foam layer ($h_f \sim 3$ mm) was sandwiched between two symmetrically pre-cracked Al_2O_3 layers ($h_c = 2$ mm). This geometry was used to study constrained tensile deformation of the foam layers.

Table 1
The relative density (σ/σ_s (-)), cell size and cell wall thickness of the Al alloy foams

Material	Code	Relative density	Cell size (mm)	Cell wall thickness (μm)
Al-12Si-0.6Mg	FC	0.23 ± 3	1.1 ± 0.4	92 ± 26
Al-1Mg-0.6Si	FW	0.21 ± 4	1.3 ± 0.6	141 ± 62

2.2. Fabrication

The laminates were prepared by hot pressing, in vacuum, alternate layers of the two constituents, at temperatures of 605 °C (FC) or 630 °C (FW). Prior to bonding, the metal mating surfaces were lightly ground on both sides to remove oxide scale and ensure macroscopic flatness. Bonding was carried out in 10^{-5} mbar vacuum, under a uniaxial pressure of 1 MPa.

2.3. Mechanical testing

Mechanical loading, including tension, three-point flexure and static indentation were conducted using a servo-hydraulic testing apparatus equipped with a 10 kN load cell.

2.3.1. Tension

A number of tests were conducted in tension. These included tests on foamed metal specimens to obtain the unconstrained stress–strain response, tests on pre-cracked sandwich specimens in order to explore the constrained deformation of the ductile layers, and tests on laminates to investigate the in-plane response. All tests were carried out under displacement control at a rate of 0.2 mm min^{-1} . The specimens were instrumented with an Instron extensometer (11.2 mm gauge length) for measuring axial strains. Tensile specimens were electro-discharge machined from the foam material. The geometry employed was a rectangular, dog-bone shape with gauge sections measuring 8 mm long, 8 mm wide and 9 mm thick. The ends of the foam specimens were vacuum infiltrated with a low viscosity resin in order to prevent crushing in the grip sections.

Model experiments [12] based on ductile bridging were conducted to quantify the work of fracture of the foamed metal layers. The geometry utilised, which is illustrated in Fig. 2 comprises a central foamed metal layer surrounded by two symmetrically pre-cracked Al_2O_3 layers. The objective was to create a sharp pre-crack (initial crack opening, u_0) in order to simulate accurately the situation that occurs in laminate fracture, where failure proceeds by crack tunnelling in the ceramic layers leaving intact metal layers in the crack wake. This was achieved by placing a row of Vickers indents along the central plane normal to the specimen axis. Loading in three-point flexure, with the indentations along the line of maximum tension, caused the

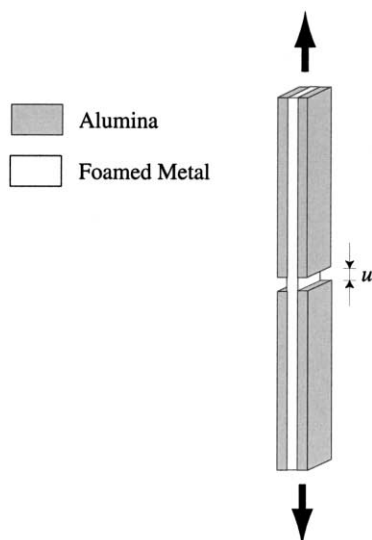


Fig. 2. Schematic illustration of a sandwich test specimen used to measure the work of fracture.

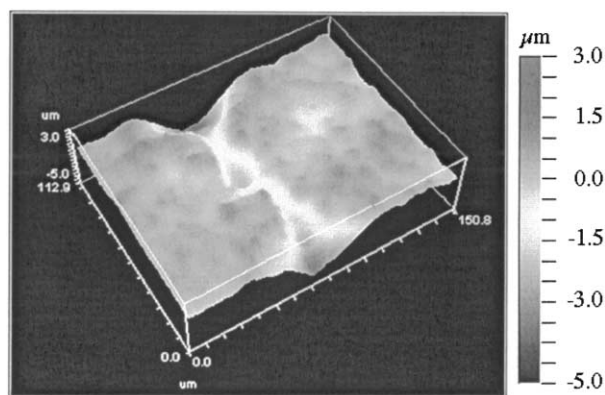


Fig. 3. Optical interferometric topography map showing the surface of the Al_2O_3 after cracking along a line of closely-spaced indents.

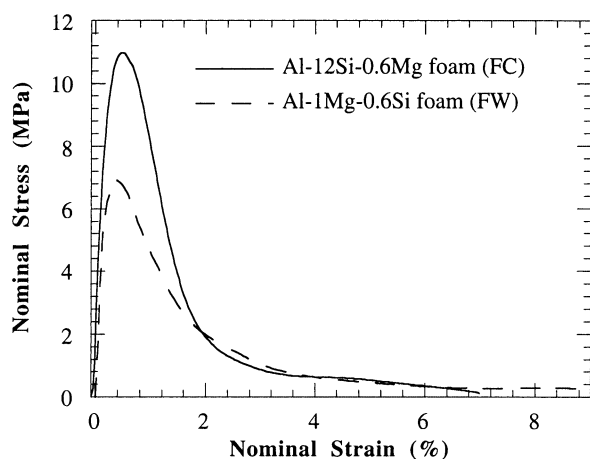


Fig. 4. Nominal stress–strain curves for unconstrained tensile loading of FC and FW foams.

formation of a sharp crack beyond the ends of the indentations. The crack extended to the Al alloy/ Al_2O_3

interface. The width of the crack, u_0 , was measured using an optical interferometric profilometer to be $23 \pm 2 \mu\text{m}$. Fig. 3 shows a topographic map of the indented and cracked surface.

2.3.2. Flexure tests

Three-point bend tests were carried out on laminates with a 35 mm loading span at a roller displacement rate of 0.02 mm min^{-1} . The tests involved loading unnotched and single face-notched beams measuring 50 mm in length and 7 mm in width. For the face-notched samples, the notch (200 μm in width) was cut traversing the outer Al_2O_3 and foam layers and rooted in the second Al_2O_3 layer. This achieved a notch depth to specimen thickness ratio of about 0.3.

2.3.3. Indenter penetration tests

Square specimens with a side length of 60 mm were cut from the bonded plates. The laminates were firmly fixed at all edges between annular clamps of 40 and 60 mm internal and external diameter, respectively. The hemispherical indenter was 10 mm in diameter and was fixed to the cross-head of a servo-hydraulic testing machine. The displacement rate was set at 1.2 mm s^{-1} .

3. Results

3.1. Unconstrained metal foams

Fig. 4 shows typical stress–strain curves obtained from tensile testing of foam specimens used as the metal constituent in the laminates. Measured yield strengths, taken as the peak stress sustained by the specimen are about 9.2 and 6.2 MPa for FC and FW, respectively. The higher strength of foam FC is largely attributable to the cell wall material being stronger. This is expected as a consequence of the presence of the Si plates in the eutectic structure, but it may also be partly associated with the oxide content being higher (Table 2).

3.2. Constrained metal foams

Fig. 5 shows typical stress–displacement curves measured for constrained FC and FW layers. The axes are the dimensionless variables σ_n/σ_Y and $2u/h_f$, where σ_n is

Table 2

Hardness values for the cell wall materials of the two foams, as obtained by nanoindentation and measured oxygen contents

Material	Hardness (GPa)	O ₂ content (%)
Al-12Si-0.6Mg (F1)	1.10 ± 0.3	1.95 ± 0.2
Al-1Mg-0.6Si (F2)	0.59 ± 0.1	0.94 ± 0.2

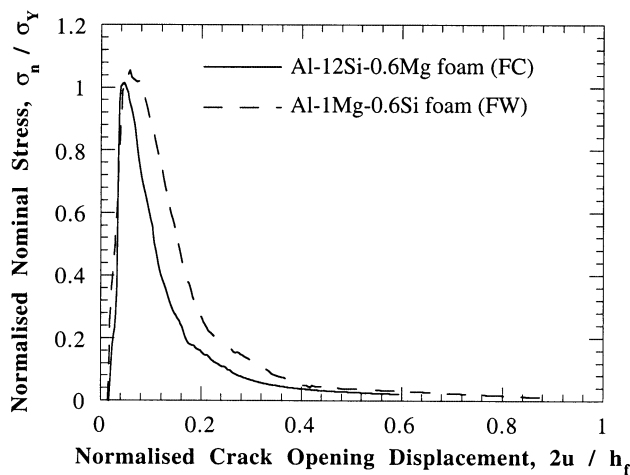


Fig. 5. Experimental data obtained during constrained tensile testing showing the nominal stress as a function of crack opening displacement for FC and FW.

the nominal stress carried by the constrained layer, σ_Y the uniaxial yield strength, u the crack opening displacement and $h_f/2$ the semi-thickness of the constrained foam layer. The curves show a rising part up to a maximum stress ratio, after which the value decays in an approximately exponential fashion giving a post-peak tail similar to that in the unconstrained state. Both foams develop peak stresses only slightly greater than the uniaxial yield strength, so that the values are considerably lower than those measured for the corresponding dense alloys [13]. This is a consequence of the limited degree to which constraint can be imposed on metallic foams which arises from relaxation of the normal stress at all the internal free surfaces (pores). Beyond the peak, the stress ratio decreases gradually down to zero at normalised critical openings, $2u^*/h_f$ of approximately 0.5 and 0.9, respectively, for FC and FW. The ‘work of fracture’, w , measured as the area under the normalised curve was equal to 0.10 and 0.17 for FC and FW foamed metal layers, respectively. The greater energy absorption for FW is attributable to the higher cell wall ductility, which can in turn be related to the cell wall microstructure [11].

3.3. In-plane laminate response

3.3.1. Tensile tests

The laminates for tensile testing were sideways notched with the notch tip incident upon the first foam layer. Notching pre-determined the failure site and allowed the crack opening displacement at the notch region to be monitored using extensometry. Typical load–displacement curves for laminates with two different foam volume fractions, $f_f (= h_f/(h_f + h_c))$ are plotted in Fig. 6.

¹ Since the laminates were composed of four ceramic layers and only three foamed metal layers, the overall metal content is slightly lower than these values.

In general, the curves display a steeply rising part up to a maximum, followed by a continuous load decrease. At the peak load, the Al_2O_3 layers included between the notches fail at some location close to the notch plane, leaving the foamed metal layers bridging the crack. Thereafter, the load supported entirely by the ductile layers exhibits a continuous decrease until final rupture. For FC/ Al_2O_3 laminates (Fig. 6(a)) prior to load maximum, a load drop occurs, indicative of damage initiating within one of the Al_2O_3 layers and warning of impending failure.

3.3.2. Flexural tests

In FC/ Al_2O_3 laminates (Fig. 7(a)) the load–displacement plots show an initial linear response followed by a first load drop. At this point, the innermost compressively-stressed ceramic layer cracked, though all the other Al_2O_3 layers remained intact. Further deflection causes the load to increase non-linearly to a distinct load drop. Direct in-situ observations of specimens at this point revealed that cracks had been formed in all the remaining ceramic layers. Further beam deflection leads to a progressive load decrease corresponding to plastic deformation of the foamed metal layers. The FW/ Al_2O_3 layered system (Fig. 7(b)) exhibits essentially the same features as the FC/ Al_2O_3 system. Flexure tests were also conducted on single face-notched laminates. The basic features of the load–deflection curves for the notched laminates are similar to those for the unnotched ones.

3.3.3. Fracture energy predictions

Estimation of the fracture energy in units $kJ m^{-2}$ involves obtaining the area under the load–displacement curves and then dividing by the fracture cross-section. This normalisation of the energy values has a valid physical meaning, since fracture tends to be localised close to a specific plane (see Fig. 12). The results are summarised in Fig. 8. It shows that energy absorption increases with increasing thickness of the foam layer (the Al_2O_3 layers have constant thickness). This is a direct consequence of the increased volume of metal, which deforms (per unit sectional area) as the distance between the ceramic layers is scaled up. Energy absorption was found to be higher for the FW/ Al_2O_3 laminates which is attributable to the FW foam tending to fail in a more ductile fashion than the FC foam.

When small scale bridging conditions are applicable, the incremental toughening of the composite for a ductile ligament can be related to the work of stretching and fracture of the bridging ligament (Eq. (1)) [14,15]. Thus, the fracture energy of the composite, G_{tot} , can be calculated from the constrained single foam layer model using the expression

$$G_{tot} = G_{cer}(1 - f_f) + f_f \sigma_Y \left(\frac{h_f}{2} \right) w \quad (1)$$

The first term on the right-hand side of Eq. (1)

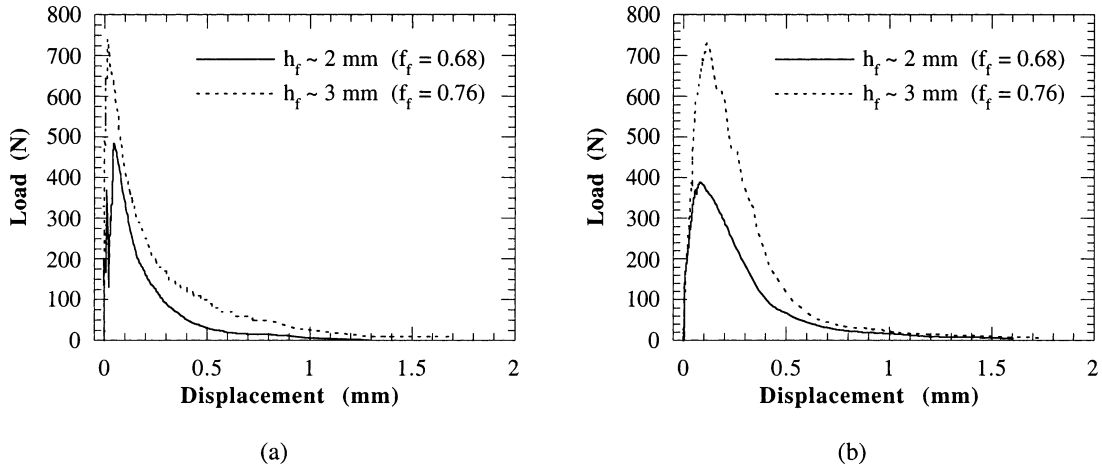


Fig. 6. Tensile load-displacement for (a) FC/Al₂O₃ and (b) FW/Al₂O₃ double face-notched laminates. The Al₂O₃ layers have a constant thickness, h_c , of 1 mm.

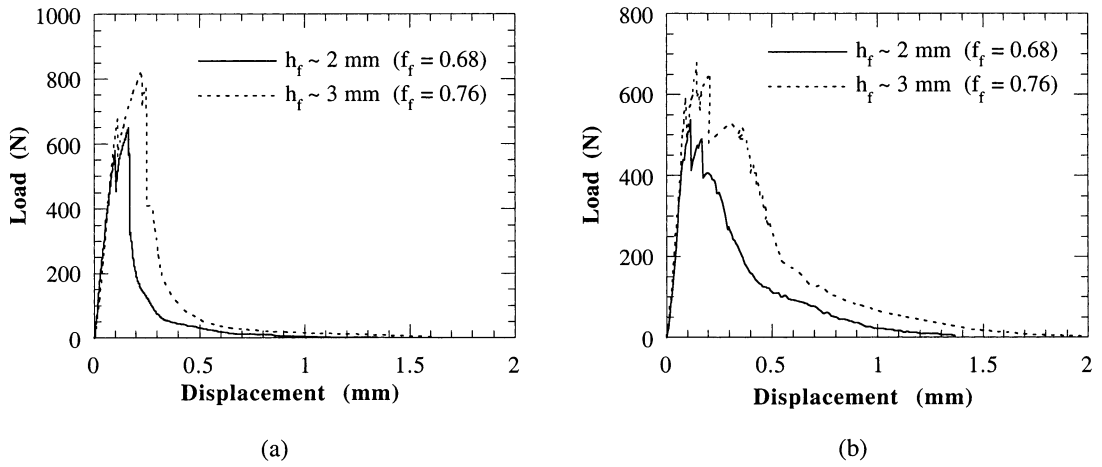


Fig. 7. Flexural load-displacement plots for unnotched laminates (a) FC/Al₂O₃ and (b) FW/Al₂O₃. The Al₂O₃ layers have a constant thickness, h_c , of 1 mm.

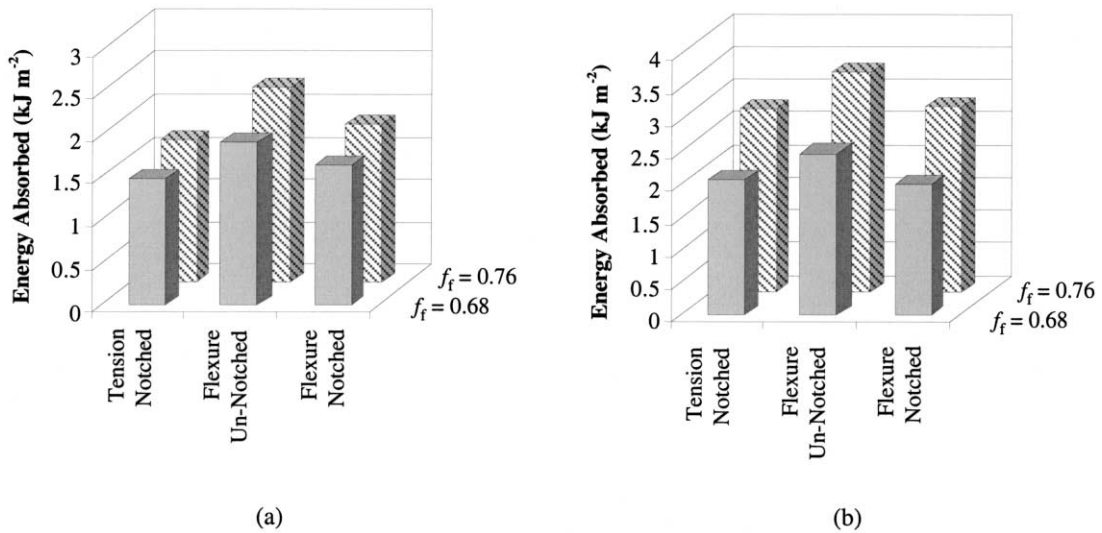


Fig. 8. Energy absorption values for (a) FC/Al₂O₃ and (b) FW/Al₂O₃ laminates tested in tension and flexure.

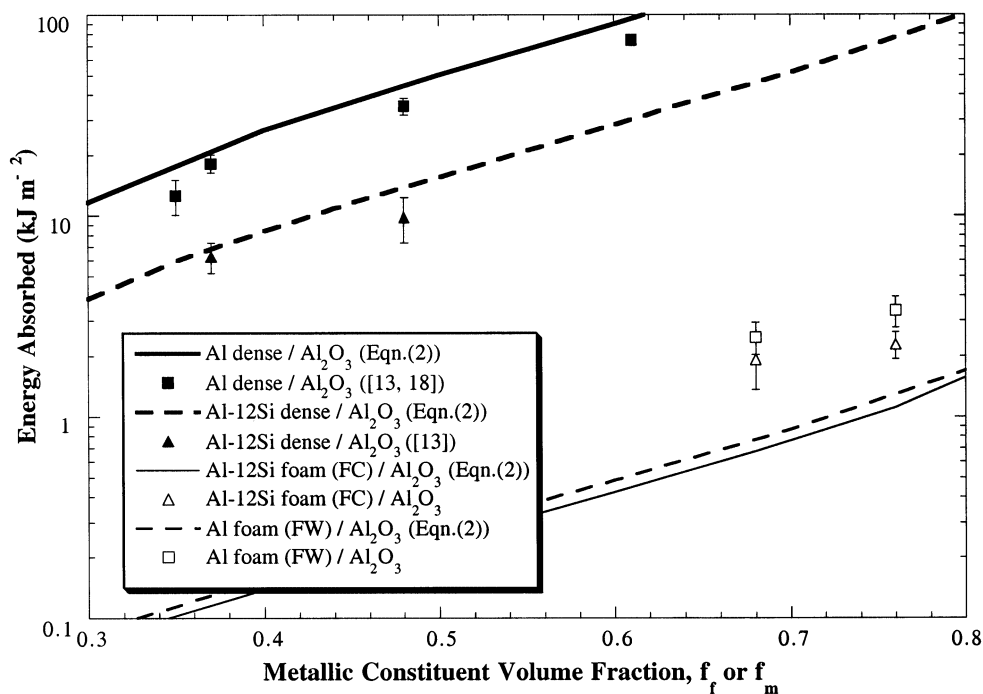


Fig. 9. Comparison between predicted and experimentally measured fracture energy of foam laminates. Experimental data were obtained from laminate flexure. Predictions are based on the work of stretching the bridging ligaments. Experimental and predicted fracture energies for the corresponding dense metal laminates are also shown.

represents the contribution from ceramic fracture, wherein G_{cer} is the fracture energy of the ceramic. Commonly, it represents only a very small contribution. According to Eq. (1), fracture energy rises with h_f . The dependence is approximately quadratic since both h_f and f_f rise when h_c is fixed. As stated previously, this equation is applicable when the cracking pattern of the composite is governed by a small-scale yielding stress field such as in the case of single crack propagation. Expressing the second term on the right-hand side in terms of the foam volume fraction, f_f , it becomes

$$G_{tot} = G_{cer}(1 - f_f) + \frac{w}{2} h_c \sigma_Y \left(\frac{f_f^2}{1 - f_f} \right) \quad (2)$$

The fracture energy of polycrystalline Al_2O_3 , G_{cer} , has been estimated [16] at between 10 and 100 $J m^{-2}$, depending on the crack length. In the current study, a constant value of 25 $J m^{-2}$ has been taken [17]. Tests on constrained tensile fracture of FC and FW foams (Section 3.2) gave an average work of fracture, w equal to 0.10 and 0.17, respectively. The value of h_c was constant in all the experiments at 1 mm. It can be seen from Fig. 4 that there is little or no work hardening so the flow stresses were taken as constant ($\sigma_{Y(FC)} = 9.2$ MPa and $\sigma_{Y(FW)} = 6.2$ MPa). The fracture energies of the foam/ceramic layered systems are thus given by the following expressions

$$G_{tot(FC)} = 25(1 - f_f) + 460 \left(\frac{f_f^2}{1 - f_f} \right) \quad (3)$$

$$G_{tot(FW)} = 25(1 - f_f) + 527 \left(\frac{f_f^2}{1 - f_f} \right) \quad (4)$$

Fig. 9 compares experimental data with predictions obtained using Eq. (2). While the trends in foam content and strength (yield stress) are correctly predicted, the experimental values for the foam-based laminates are greater than the theoretical ones by a factor of about three. This may be partly attributable to a contribution from interfacial debonding, although, since the interfacial fracture energies are relatively low (less than 40 $J m^{-2}$) [13], this is not really expected to be very significant. However, interfacial debonding may have led to significant work being done by frictional sliding as the crack opens up, particularly in view of the fact that the measurements were made in bending which can accentuate the interference between the crack flanks as they disengage. Also shown on the plot are the experimental and predicted fracture energies for the corresponding dense metal laminates. In this case, the experimental fracture energies are slightly lower than the predicted values. In view of the greater toughness, any contribution from frictional sliding is expected to be much less significant in these cases.

3.3.4. Cracking pattern

In metal/ceramic laminates, there is a critical metal volume fraction (typically less than 0.5) above which failure switches from single to multiple cracking mode within the ceramic layers. Multiple cracking signifi-

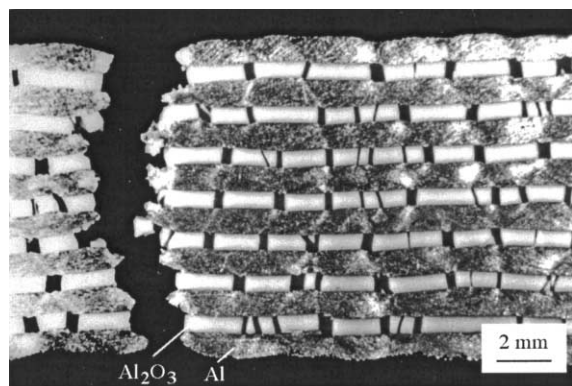


Fig. 10. Typical multiple cracking pattern [14] in an Al/Al₂O₃ multi-layer composite with $f_f = 0.68$.

cantly enhances the fracture energy, since energy dissipation by metal plasticity occurs in several locations of each metal layer (although usually only one of them stretches to failure). A typical example of such a failure is illustrated in Fig. 10 for an Al/Al₂O₃ laminate with 68% metal [4]. Theoretically [19], it is predicted that the multiple cracking mode is expected if the metal layer thickness is 2.5 times larger than the ceramic layer thickness (Fig. 11). This corresponds to a metal volume fraction of 0.7. Predictions are in fairly good agreement with experimental results [18–20] obtained for various layered systems.

In the present study, laminates with foam volume fraction² in the range of 0.6–0.8 always failed through

² Equivalent metal volume fractions, assuming that the pores have disappeared, are between 0.33 and 0.6.

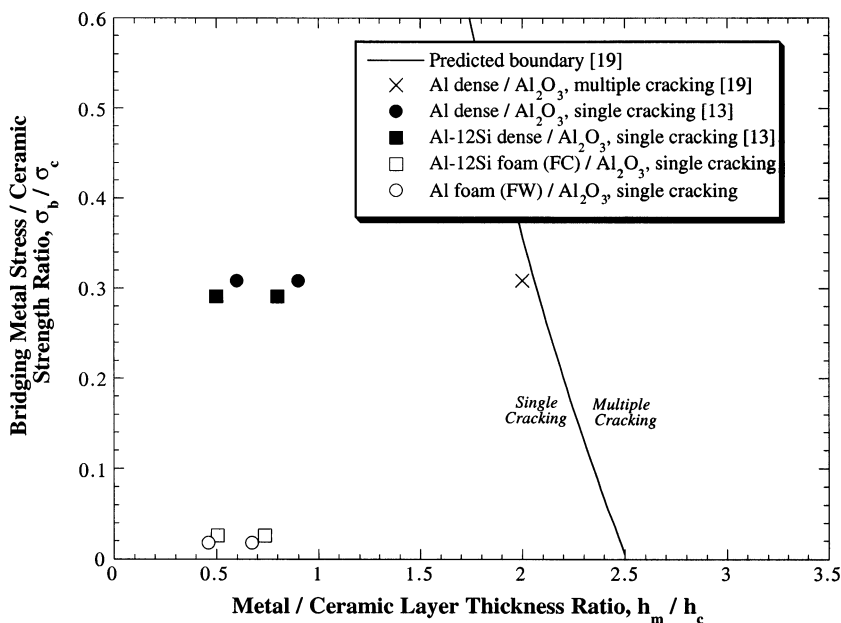


Fig. 11. Plot of the ratio of bridging metal stress to ceramic strength against the metal/ceramic layer thickness ratio. The mean fracture strength of the Al₂O₃ layers, measured using three-point bend tests is 375 MPa. The solid curve of the LEM model [19] separates the single cracking regime from that of multiple cracking. Experimental data obtained from dense and foamed metal/ceramic laminates are also shown.

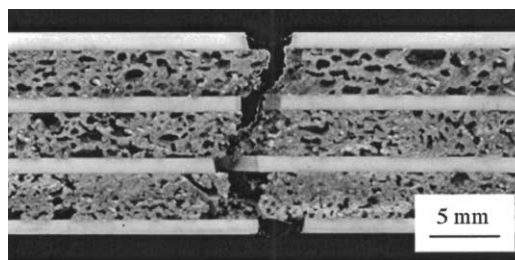


Fig. 12. Crack path in an FC/Al₂O₃ laminate.

the propagation of an approximately planar crack, i.e. single, dominant cracking mode, as illustrated in Fig. 12. Hence, the stress in the uncracked ceramic layer ahead of the crack was always higher than that in the crack wake [20]. The values of metal bridging stress to ceramic strength ratio, σ_b / σ_c , for metallic foam/ceramic laminates are shown in Fig. 11 versus the metal/ceramic layer thickness ratio, h_m / h_c (excluding voids). Also, for comparison, the corresponding data for dense metal laminates are shown. According to prediction [19], the critical h_m / h_c ratio above which multiple cracking occurs increases as the σ_b / σ_c ratio decreases. Thus, the critical metal volume fraction will be higher for the foam laminates than for the dense metal laminates. If this is the case, multiple cracking will only be stimulated once the scale of the structure increases substantially (very high foam volume fractions), which in turn may conflict with other aims such as overall thickness limitations.

However, it is possible that this transition will not occur even at very high volume fractions of metal. For

multiple cracking to occur, the stresses within the cracked Al_2O_3 layers need to build up to substantial levels in order to shift the location of maximum stress from the crack tip to the crack wake. This in turn requires that the interface which controls the degree of stress transfer between the metal and the ceramic must be sufficiently strong [21]. Moreover, the foamed metal layers must have sufficient strength and ductility to bridge the cracks formed in the brittle layers without failing prematurely [6]. However, the foam/ceramic interface is relatively ‘weak’ as a consequence of the low contact area associated with the foam. Also the foam strength is relatively low (although this is dependent on the cell wall microstructure and this was far from optimal in the foams studied here).

On the other hand, the greater spacing between the ceramic layers for a given metal/ceramic ratio (excluding voids) which are created with foams may favour multiple cracking by reducing the stress concentrating effect at the crack tip. The net effect is difficult to

predict theoretically, but multiple cracking has certainly not been observed with the geometries employed here and it seems likely that it will be difficult to stimulate in metallic foam/ceramic laminates. It should, however, be mentioned that ‘foams’ with much lower void contents might be produced such that multiple cracking would be possible.

3.4. Indenter penetration

A comparison has been made between the penetration response of $\text{FC}/\text{Al}_2\text{O}_3$ and $\text{FW}/\text{Al}_2\text{O}_3$ plates of similar areal density ($\sim 20 \text{ kg m}^{-2}$). Fig. 13 gives typical force–displacement curves for the two laminate systems with two different foam layer thickness. The damage area and the energy absorbed per unit volume of damaged material are compared in Fig. 14. The energy absorption values have been calculated by dividing the energy (area under the force–displacement curve) by the product of damage area and indentation

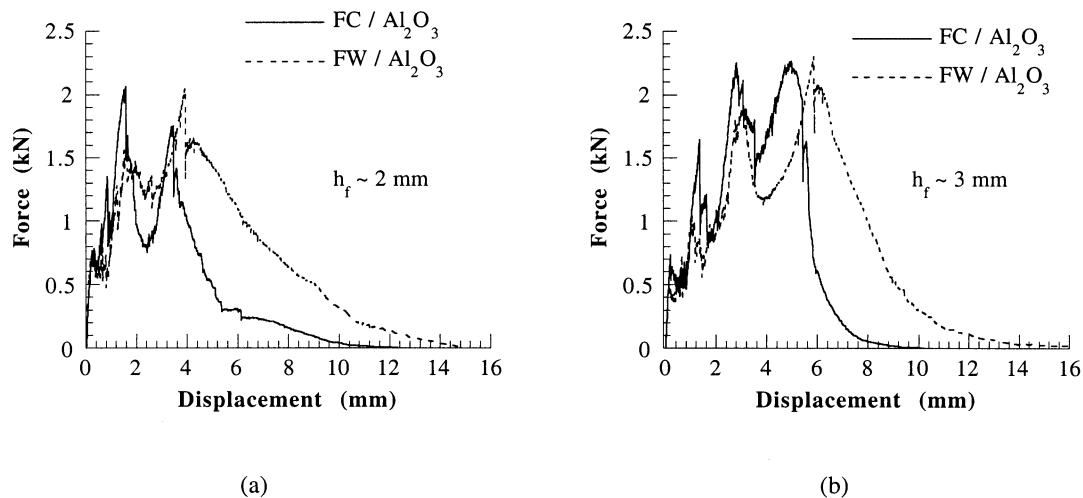


Fig. 13. Typical force–displacement responses measured during quasi-static indentation, for $\text{FC}/\text{Al}_2\text{O}_3$ and $\text{FW}/\text{Al}_2\text{O}_3$ laminates with two different foam layer thicknesses (a) $h_f \sim 2 \text{ mm}$ and (b) $h_f \sim 3 \text{ mm}$. The Al_2O_3 layers have a constant thickness, h_c , of 1 mm.

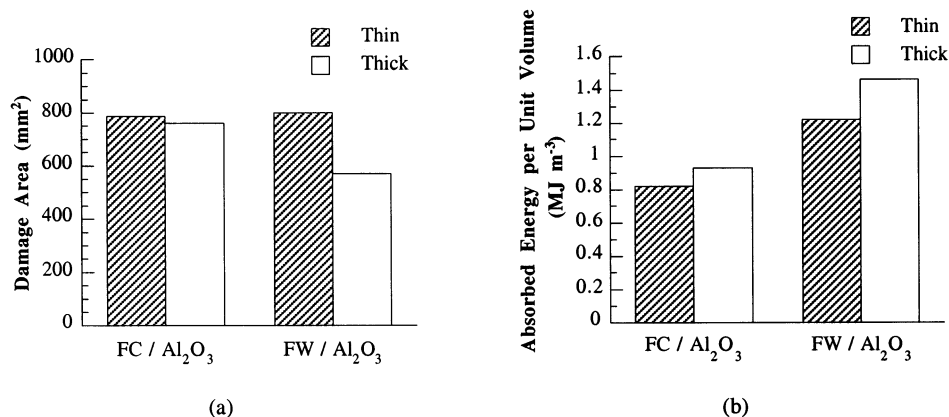


Fig. 14. (a) Damage area; and (b) energy absorption per unit volume for $\text{FC}/\text{Al}_2\text{O}_3$ and $\text{FW}/\text{Al}_2\text{O}_3$ laminates.

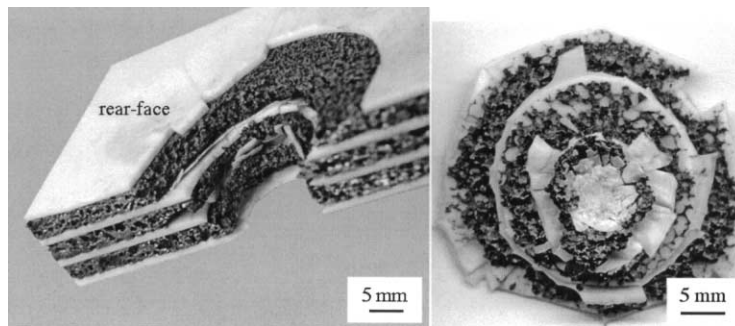


Fig. 15. Penetrated FC/Al₂O₃ laminate and the plug ejected.

depth. The extent of damage has been measured by projecting damage areas at all interfaces onto a single plane, and thus the energy absorption results in Fig. 14 represent lower bounds. It is evident that FW/Al₂O₃ laminates absorb more energy per unit volume than FC/Al₂O₃ laminates. In order to explain this disparity the macroscopic mechanism of penetration for the two systems was considered. In FC/Al₂O₃ plates, the indenter readily penetrates the laminate punching out a plug from the distal side (Fig. 15). In FW/Al₂O₃ plates on the other hand no plug is removed and there is significant bulging of the rear surface of the target, as illustrated in Fig. 16.

Comparing the force–displacement responses for the two laminates in Fig. 13 it can be seen that the penetration energy (area under the force–displacement curve) of the FW/Al₂O₃ laminates is higher, which may represent the energy absorbed in bulging the rear surface of the plate. Also additional energy dissipation may occur in moving the material ahead of the indenter along with it due to friction between the indenter and the plate material.

4. Conclusions

A study has been made of the failure mechanisms in metal foam/ceramic laminates. The main conclusions are:

1. Tensile loading of single metallic foam layers sandwiched between pre-cracked ceramic layers gave a peak at low displacement, followed by a progressive drop to zero as rupture occurred. The loads expressed as a nominal stress and normalised by the yield stress of corresponding unconstrained foam, peak at values close to unity, so that constraint generates minimal strengthening from stress triaxiality. This is consistent with stress relaxation around pores reducing the constraint effect. While in principle, reductions in constraint may promote plastic flow in a larger volume of metal, this did not occur with the foams used and localisation of strain around pores led to premature rupture. This is at

least partly attributed to the cell wall material in both of the foams studied exhibiting relatively low ductility and toughness.

2. In-plane tensile loading and bending have been carried out on foam/ceramic laminates in order to explore the fracture behaviour and measure the fracture energy. Laminates made from a dilute alloy foam (FW) exhibited larger strains to failure and greater energy absorption than those made from an Al–Si eutectic alloy (FC). This is attributed to the greater ductility of the cell wall material in the FW foam. Comparison between measured fracture energies and those predicted using a previously developed model based on the work done during stretching of bridging ligaments, showed good agreement in terms of the effects of foam content and foam strength. The absolute values, which are considerably lower than those for corresponding dense metallic layers are of the right order of magnitude. However, the experimental values are appreciably higher than the predicted ones. This may arise from frictional sliding between crack flanks as they disengage.
3. Multiple cracking which can be stimulated in laminates made from dense metallic layers has not been observed with foam laminates. This is consistent with model predictions, which indicate that the strength of the foam would have to be raised substantially in order for multiple cracking to occur.
4. A comparison has been made between the responses of FC and FW laminates to penetration of a hemi-



Fig. 16. Cross-section of a penetrated FW/Al₂O₃ laminate, the surface initially struck by the indenter being at the bottom. Bulging of the rear surface of the target is evident.

spherical indenter. The FW laminates required higher penetration energies than the FC laminates. This is attributed to a greater cell wall ductility which gave rise to different macroscopic mechanisms of penetration.

5. The study has highlighted certain inherent limitations in the mechanical performance of laminates composed of alternate ceramic and metal foam layers, particularly relating to the effects of low triaxial constraint and difficulties in generating multiple cracking. It is also clear that for use in laminates and in other configurations metal foams are required in which the microstructure of the cell wall is such that its ductility and toughness are higher than those of currently available materials.

Acknowledgements

This work forms part of an initiative concerning metallic foams and associated sandwich and multi-layer structures, which is partially supported by EPSRC. Support for A.E.M. via the State Scholarships Foundation (SSF) of Greece is gratefully acknowledged.

References

- [1] M.C. Shaw, D.B. Marshall, A.G. Evans, *Mater. Res. Soc. Symp. Proc.* 170 (1990) 25–31.
- [2] Z. Chen, J.J. Mecholsky, *J. Mater. Res. Soc.* 8 (1993) 2362–2369.
- [3] S.K. Pateras, M.C. Shaw, W.I. Clegg, A.C.F. Cocks, T.W. Clyne, in: A. Poursartip, K. Street (Eds.), 10th International Conference on Composite Materials (ICCM10), Whistler, Woodhead City, BC, Canada, 1995, pp. 731–737.
- [4] S.J. Howard, S.K. Pateras, T.W. Clyne, *Mater. Sci. Technol.* 14 (1998) 535–541.
- [5] K.L. Hwu, B. Derby, *Acta Mater.* 47 (1999) 545–563.
- [6] M.C. Shaw, *Comprehensive Composite Materials*, in: T.W. Clyne (Ed.), *Metal Matrix Composites*, vol. 3, Elsevier, Amsterdam, 2000 Chapter 3.11.
- [7] D. Sherman, D.G. Brandon, *J. Mater. Res.* 12 (1997) 1335–1343.
- [8] A. Haque, A. Abutalib, K. Rahul, U.K. Vaidya, H. Mahfuz, S. Jeelani, T. Massard, A. Vautrin, 12th International Conference on Composite Materials (ICCM-12), 1999, Paris, France, Woodhead City, paper 481.
- [9] A.E. Markaki, T.W. Clyne, *Mater. Sci. Technol.* 16 (2000) 785–791.
- [10] F. Simancik, H.P. Degischer, H. Wörz, 4th European Conference on Advanced Materials & Processes (Emomat 95), Assoc Italian de Metall, Venice/Padua, Italy, 1995, pp. 191–196.
- [11] A.E. Markaki, T.W. Clyne, *Acta Mater.* (2001) in press.
- [12] M.F. Ashby, F.J. Blunt, M. Bannister, *Acta Metall.* 37 (1989) 1847–1857.
- [13] A.E. Markaki, Ph.D Thesis, University of Cambridge, Cambridge, (2000).
- [14] L.S. Sigl, P.A. Mataga, B.J. Dalgleish, R.M. McMeeking, A.G. Evans, *Acta Metall. Mater.* 36 (1988) 945–953.
- [15] A.G. Evans, *J. Am. Ceram. Soc.* 73 (1990) 187–206.
- [16] G. Vekinis, M.F. Ashby, P.W.R. Beaumont, *Acta Metall. Mater.* 38 (1990) 1151–1162.
- [17] B.D. Flinn, F.W. Zok, F.F. Lange, A.G. Evans, *Mater. Sci. Eng. A* 144 (1991) 153–157.
- [18] S. Pateras, Ph.D. Thesis, University of Cambridge, Cambridge (1997).
- [19] Y. Huang, H.W. Zhang, *Acta Metall. Mater.* 43 (1995) 1523–1530.
- [20] M.C. Shaw, D.B. Marshall, M.S. Dadkhah, A.G. Evans, *Acta Metall. Mater.* 41 (1993) 3311–3320.
- [21] M.C. Shaw, *Key Eng. Mater.* 116 (1996) 261–278.